

Article

Effect of Si and Zr on the Microstructure and Properties of Al-Fe-Si-Zr Alloys

Anna Morozova ¹, Anna Mogucheva ^{1,*}, Dmitriy Bukin ¹, Olga Lukianova ¹, Natalya Korotkova ², Nikolay Belov ²  and Rustam Kaibyshev ¹

¹ Laboratory of Mechanical Properties of Nanostructured Materials and Superalloys, Belgorod State University, Belgorod 308015, Russia; morozova_ai@bsu.edu.ru (A.M.); bukin-15@mail.ru (D.B.); lukyanova_oa@bsu.edu.ru (O.L.); rustam_kaibyshev@bsu.edu.ru (R.K.)

² Department of Casting Technologies, Moscow Institute of steel and Alloys, Moscow 119049, Russia; darkhopex@mail.ru (N.K.); nikolay-belov@yandex.ru (N.B.)

* Correspondence: mogucheva@bsu.edu.ru; Tel.: +7-4722-585417

Received: 10 October 2017; Accepted: 8 November 2017; Published: 11 November 2017

Abstract: The effects of Si and Zr on the microstructure, microhardness and electrical conductivity of Al-Fe-Si-Zr alloys were studied. An increase in the Zr content over 0.3 wt. % leads to the formation of primary Al₃Zr inclusions and also decreases mechanical properties. Therefore, the Zr content should not be more than 0.3 wt. %, although the smaller content is insufficient for the strengthening by the secondary Al₃Zr precipitates. The present results indicate that high content of Si significantly affects the hardness and electrical conductivity of the investigated alloys. However, the absence of Si led to the formation of harmful needle-shaped Al₃Fe particles in the microstructure of the investigated alloys after annealing. Therefore, the optimum amount of Si was 0.25–0.50 wt. % due to the formation of the Al₈Fe₂Si phase with the preferable platelet morphology. The maximum microhardness and strengthening effects in Al-1% Fe-0.25% Si-0.3% Zr were observed after annealing at 400–450 °C due to the formation of nanosized coherent Al₃Zr (L1₂) dispersoids. The effect of the increasing of the electrical conductivity can be explained by the decomposition of the solid solution. Thus, Al-1% Fe-0.25% Si-0.3% Zr alloy annealed at 450 °C has been studied in detail as the most attractive with respect to the special focus on transmission line applications.

Keywords: aluminum alloys; Al-Fe-Si-Zr system; microstructure; hardness; electrical conductivity

1. Introduction

Al-Fe-Si alloys belonging to the 1XXX series are commonly used in a wide range of different applications including electrical conductors [1]. The fruitful combination of the light weight and reasonable electrical conductivity makes these alloys preferable for the production of wires for overhead power transmission lines compared with Cu [2]. The high electrical conductivity of these alloys approaching the theoretical limit for Al of 62% IACS (The International Annealed Copper Standard defines 17.241 nm as 100%) is attributed to the very low solubility of Si and Fe in aluminum. The tensile properties of these alloys are low. At present, there is a strong requirement for increased strength and thermal stability of Al alloys used for transmission lines. These alloys have to withstand a high operating temperature of ~150°. Such a transition metal as Zr is used to improve the strength at room temperature and to provide the retention of the structure and tensile properties at elevated temperatures due to the formation of Al₃Zr dispersoids during homogenizing treatment [2]. Zr is one of the most promising additives for developing castable, precipitation-hardened alloys with good coarsening and creep resistance and usually used as a recrystallization inhibitor and grain refiner in commercial Al alloys. In addition, the solubility of this alloying element in Al

is negligible, and therefore, Al-Zr alloys may exhibit high strength, thermal stability and electrical conductivity, concurrently.

A detailed description of the ternary Al-Fe-Si phase diagram can be found in [3]. It is possible to expect the formation of such equilibrium intermetallics as $\text{Al}_{13}\text{Fe}_4$ (θ phase), Al_3Fe phase, α -AlFeSi and β -AlFeSi via peritectic (θ and α -AlFeSi) or eutectic (β -AlFeSi) reactions in the aluminum corner of the equilibrium Al-Fe-Si phase. It is known that needle-shaped Al_3Fe particles dramatically decrease the technological ductility of aluminum alloys [3]. The content of Si is added to prevent suppression of Al_3Fe particles formation and to provide the α -AlFeSi ($\text{Al}_8\text{Fe}_2\text{Si}$) and β -AlFeSi (Al_5FeSi) phases' precipitation into these alloys [3]. However, there is very limited information in the literature on the effectiveness of the influence of Si and Zr on the structure and properties in these alloys. β -AlFeSi is the most harmful phase decreasing the mechanical properties of Al alloys as described in [4]. There are three major types of β -AlFeSi intermetallics with orthorhombic, tetragonal and monoclinic crystal structures. As described in [5], such elements as Mn, Co, Sr or reduction of the solidification rate are widely used to form the α -AlFeSi preferred phase.

Al_3Zr may exist in three main forms: the stable, tetragonal (D_{023}) modification, the metastable cubic (L_{12}) modification and in the primary form. Increased Zr content or casting defects can lead to the formation of the primary Al_3Zr inclusions. However, a significant precipitation hardening can be provided by a very small addition of Zr. This can be explained by the precipitation of metastable Al_3Zr particles during post-solidification heat treatment. The metastable Al_3Zr phase has the same structure as the Al matrix. The coherence of the metastable Al_3Zr particles with the aluminum matrix leads to better thermal stability and an appreciable precipitation hardening effect. The L_{12} structure of the metastable Al_3Zr particles transforms into the complex tetragonal D_{023} stable form after annealing at temperatures up to 500 °C [6,7]. Stable Al_3Zr precipitates are semi-coherent with the Al matrix. The growth of the metastable Al_3Zr precipitates and the loss of their coherence reduce the hardening effect. Features of the microstructure and mechanical properties of aluminum alloys with the addition of Si, Fe and various contents of Zr are described by Belov et al. [2,8–10].

At present, the implementation of the inert anode technique for the production of primary Al requires the development of a new class of Al-Fe-Si-Zr alloys, which have to combine the low cost of Al-Fe-Si alloys with the high strength and sufficient thermal stability of Al-Zr alloys. The key aim of the present study is to optimize the alloying content and the heat treatment to produce an aluminum alloy belonging to the Al-Fe-Si-Zr system with high electrical conductivity and high performance properties. The concurrent influence of Si and Zr on the microstructure, electrical conductivity and microhardness of several Al-Fe-Si-Zr alloys has been investigated. The effect of casting conditions and multistage annealing on these properties was also examined taking into account the feasibility to use these alloys for high-volume production of wires for transmission lines.

2. Materials and Methods

Experimental alloys of the Al-Fe-Si-Zr system (Table 1) were prepared in an electric furnace LAC PT 90/13 (LAC, s.r.o., Rajhrad, Czech Republic) in graphite-chamotte crucibles using 99.99% pure Al and master alloys containing 0.15 wt. %, 0.3 wt. %, 0.45 wt. % and 0.6 wt. % Zr and 0.25 wt. %, 0.5 wt. %, 0.75 wt. % and 1 wt. % Si, respectively. The casting temperature for all alloys is marked in green, and the calculated liquidus temperature (Thermo-Calc software AB, TTAL5 database, Version 5.0.4.75, Thermo-Calc Software, Stockholm, Sweden, 2010) is marked in red in Figure 1, respectively.

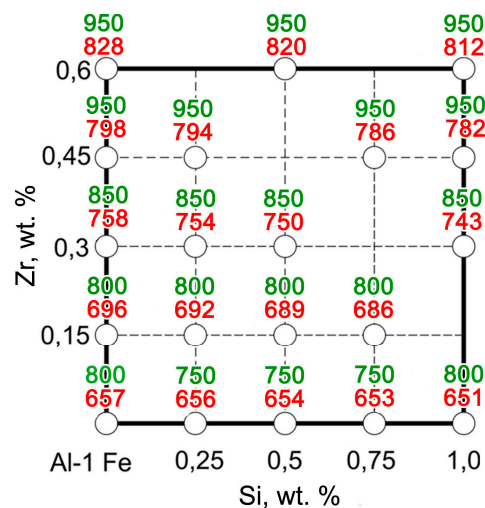


Figure 1. Quadrilateral scheme of Al-1Fe-Si-Zr.

The cast samples were annealed during 3 h in an electric furnace at a temperature ranging from 200 °C to 600 °C using stepped modes as given in Table 1.

Table 1. Annealing regimes of Al-Fe-Si-Zr alloys.

Designation	S200	S250	S300	S350	S400	S450	S500	S550	S600
Annealing regime	200 °C	S200 + 250 °C	S250 + 300 °C	S300 + 350 °C	S350 + 400 °C	S400 + 450 °C	S450 + 500 °C	S500 + 550 °C	S550 + 600 °C

The microstructures of the as-cast and homogenized samples were examined using an Axio Observer MAT and TESCAN VEGA 3 and Quanta 200 scanning electron microscopes (SEM) (FEI, Hillsboro, OR, USA). For microstructure examination, the samples were polished in a perchloric acid-ethanol electrolyte (6 C₂H₅OH/1 HClO₄/1 glycerol) and additionally oxidized in a 5% water solution of HBF₄ at constant voltage of 20 V to reveal the grain structure. Foils for transmission electron microscopy were electrolytically thinned in a perchloric acid-ethanol solution and examined using a JEOL JEM-2100 transmission electron microscope (TEM) (JEOL Ltd., Tokyo, Japan) with a double-tilt stage at 200 KV.

The electrical conductivity was measured by the method of eddy currents using a Constanta K6 device (Constanta, Sankt Peterburg, Russia). The measurements of the Vickers microhardness were performed at room temperature on metallographically-polished sections using 50-N loads and a dwell time of 15 s.

3. Results

Typical microstructures that evolved in the Al-Fe-Si-Zr alloys with different contents of Si ranging from 0 wt. % to 1 wt. % are shown in Figure 2. A eutectic included supersaturated aluminum matrix (Al) and the Al₆Fe-phase have been observed along the boundaries of dendritic cells in the considered alloys with the absence of Si (Figure 2a); while (Al) + Al₃Fe₂Si eutectic in the investigated Al alloys with 0.25–1 wt. % Si was associated with an increase in Si content, as shown in Figure 2b–d. In the Al-1% Fe-1% Si-0.3% Zr is observed the precipitating of particles (see Figure 3d), which Belov et al. [11] defined as a Si-rich inclusion. Such a precipitate decreases the electrical conductivity in aluminum alloys [12].

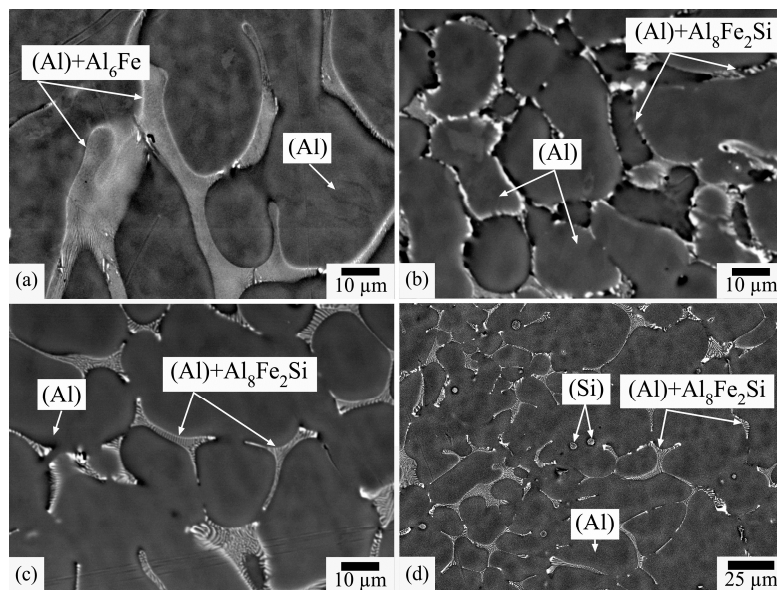


Figure 2. Microstructure of as-cast alloys with different contents of Si: (a) Al-1% Fe-0.3% Zr; (b) Al-1% Fe-0.25% Si-0.3% Zr; (c) Al-1% Fe-0.5% Si-0.3% Zr; (d) Al-1% Fe-1% Si-0.3% Zr.

3.1. Scanning Electron Microscope

Figure 3 shows the SEM of the as-cast microstructure of Al-Fe-Si-Zr alloys with different content of Zr and fixed content of Fe 1 wt. % and Si 0.5 wt. %. The observed microstructure consists of α -Al dendrites (matrix) and different Fe-Si-rich intermetallic phases distributed along the aluminum dendrite. The microstructures of the described as-cast alloys Al-1%Fe-0.5%Si with Zr content from 0 wt. % to 0.3 wt. % were nearly the same and consist of the solid solution of aluminum (Al) and a eutectic (Al) + $\text{Al}_8\text{Fe}_2\text{Si}$ along the boundaries of dendritic cells (Figure 3a–c). Lack of the primary crystals of Al_3Zr clearly shows full incorporation of Zr into the solid solution and the optimum rate of crystallization for chemical composition. The primary Al_3Zr crystals with a cross-shaped morphology were found in the microstructure of the investigated alloys with 0.45–0.6 wt. % of Zr (Figure 3d).

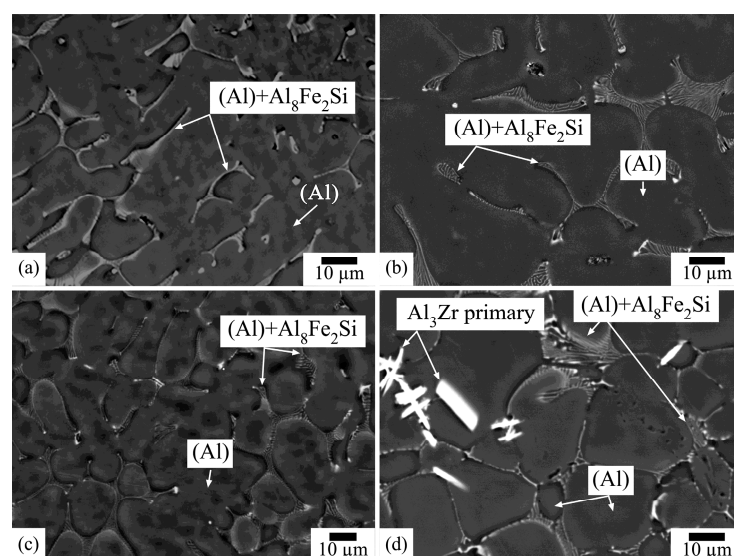


Figure 3. Microstructure of as-cast alloys with different contents of Zr: (a) Al-1%Fe-0.5%Si; (b) Al-1% Fe-0.5% Si-0.15% Zr; (c) Al-1% Fe-0.5% Si-0.3%Zr; (d) Al-1% Fe-0.5% Si-0.6% Zr.

The annealing process is a key factor that determines the objectives to produce Al alloys containing up to 0.6 wt. % Zr. Figure 4a shows that the metastable phase Al_6Fe is transformed into a stable needle-like Al_3Fe phase during the heat treatment, which considerably reduces the technological ductility, relative elongation and structural strength [11]. Therefore, the harmful needle-shaped Al_3Fe was observed in the microstructure of the investigated Al-1% Fe-0.3% Zr alloy [1]. An increase in the Si content leads to a decrease in the Al_3Fe and improvement of $\text{Al}_8\text{Fe}_2\text{Si}$ (30%–33% Fe, 6%–12% Si [3]) content, as can be seen in Figure 4b,c.

Figure 4b shows the stable D0_{23} Al_3Zr particles predominantly at the center of the dendritic cells formed as a result of transformation from the metastable Al_3Zr L1_2 particles for Al-Fe-Si-Zr alloys with 0.15 wt. % Zr during the heat treatment at the maximum annealing temperature 600 °C. The number of precipitates is lower as compared with alloys with higher Zr content.

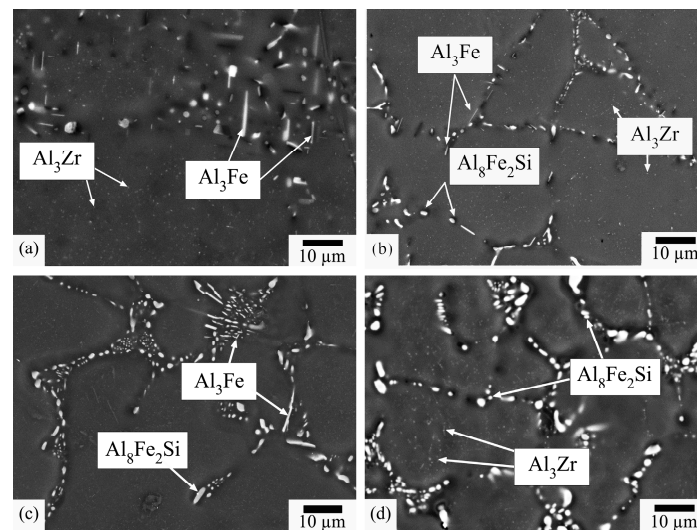


Figure 4. Microstructure of Al-1%Fe-Si-0.3%Zr alloys annealed at S600 with different contents of Si: (a) Al-1% Fe-0.3% Zr; (b) Al-1% Fe-0.25% Si-0.3% Zr; (c) Al-1% Fe-0.5% Si-0.3% Zr; (d) Al-1% Fe-1% Si-0.3% Zr.

3.2. Transmission Electron Microscope

Typical fine structures of the Al-1%Fe-0.25%Si-0.3%Zr alloy are shown in Figures 5 and 6 for the S450 peak-aging condition and the S600 overaging condition, respectively. The high magnification of SEM and TEM micrographs of the Al-Fe-Si-Zr alloys with 0.25 wt. % Si and 0.3 wt. % Zr in Figure 5 suggest that small, spheroidal, coherent Al_3Zr (L1_2) precipitates are confined to the dendritic cells, which are surrounded by precipitate-free interdendritic channels. All fine Al_3Zr (L1_2) particles inside the marked red circle in Figure 5 are characterized by a cubic structure with $a = 4.09$ and an average size of about 10 nm. The orientation relationship between the matrix and Al_3Zr (L1_2) precipitates is the cube-cube: $(020) \text{Al} \parallel (020) \text{Al}_3\text{Zr}$, $(002) \text{Al} \parallel (002) \text{Al}_3\text{Zr}$, $[022] \text{Al} \parallel [022] \text{Al}_3\text{Zr}$.

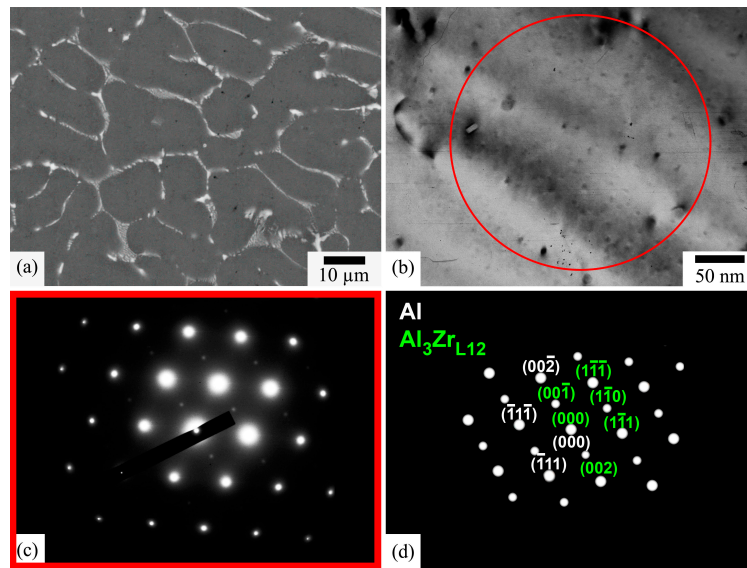


Figure 5. Transmission electron microscope (TEM) micrographs of Al-1% Fe-0.25% Si-0.3% Zr annealed at S450 with coherent L12 Al_3Zr nano-particles: (a) scanning electron microscopes (SEM); (b) TEM; (c) diffraction; (d) schematic diffraction pattern with indexes.

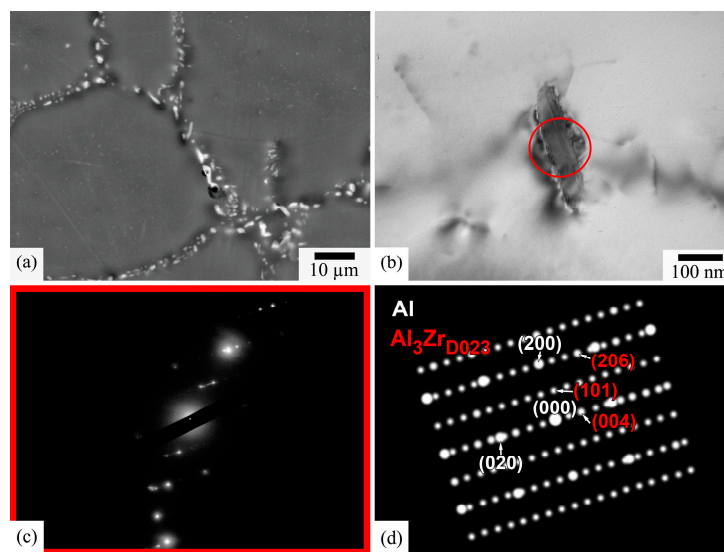


Figure 6. TEM micrographs of Al-1% Fe-0.25% Si-0.3% Zr annealed at S600 with incoherent D0_{23} Al_3Zr particles: (a) SEM; (b) TEM; (c) diffraction; (d) schematic diffraction pattern with indexes.

The annealing at S600 (Figure 6) leads to the particle growth in direction [002], and the transformation cubic L1_2 precipitates into the stable complex tetragonal D0_{23} -phase with the cell parameters $a = b = 0.3999$ nm, $c = 1.7283$ nm. The Al_3Zr (D0_{23}) is characterized by the incoherent boundaries and has an orientation relationship with the matrix: (002) Al || (020) Al_3Zr , (020) Al || (002) Al_3Zr , [100] Al || [001] Al_3Zr . A good correlation of the twice interplanar spacing (002) in aluminum ($d(002)$ Al = 0.2025 nm [13]) and interplanar spacing (001) in the Al_3Zr (D0_{23}) phase ($d(004)$ Al_3Zr = 0.4321 nm [14]) provides the particles growth along the [002] matrix direction, and the plate-like shape diameter of $\text{Al}_3\text{ZrD0}_{23}$ -particles is 250 nm, with a thickness of 50 nm.

3.3. Hardness and Electrical Conductivity

Figure 7a–d show the temperature-hardness dependences of the investigated Al alloys after annealing at different temperatures. It is shown that the shapes of the curves were typical and the same in all cases. The Si content led to improved hardness in the alloys. On the other hand, an increase in the annealing temperature decreased hardness.

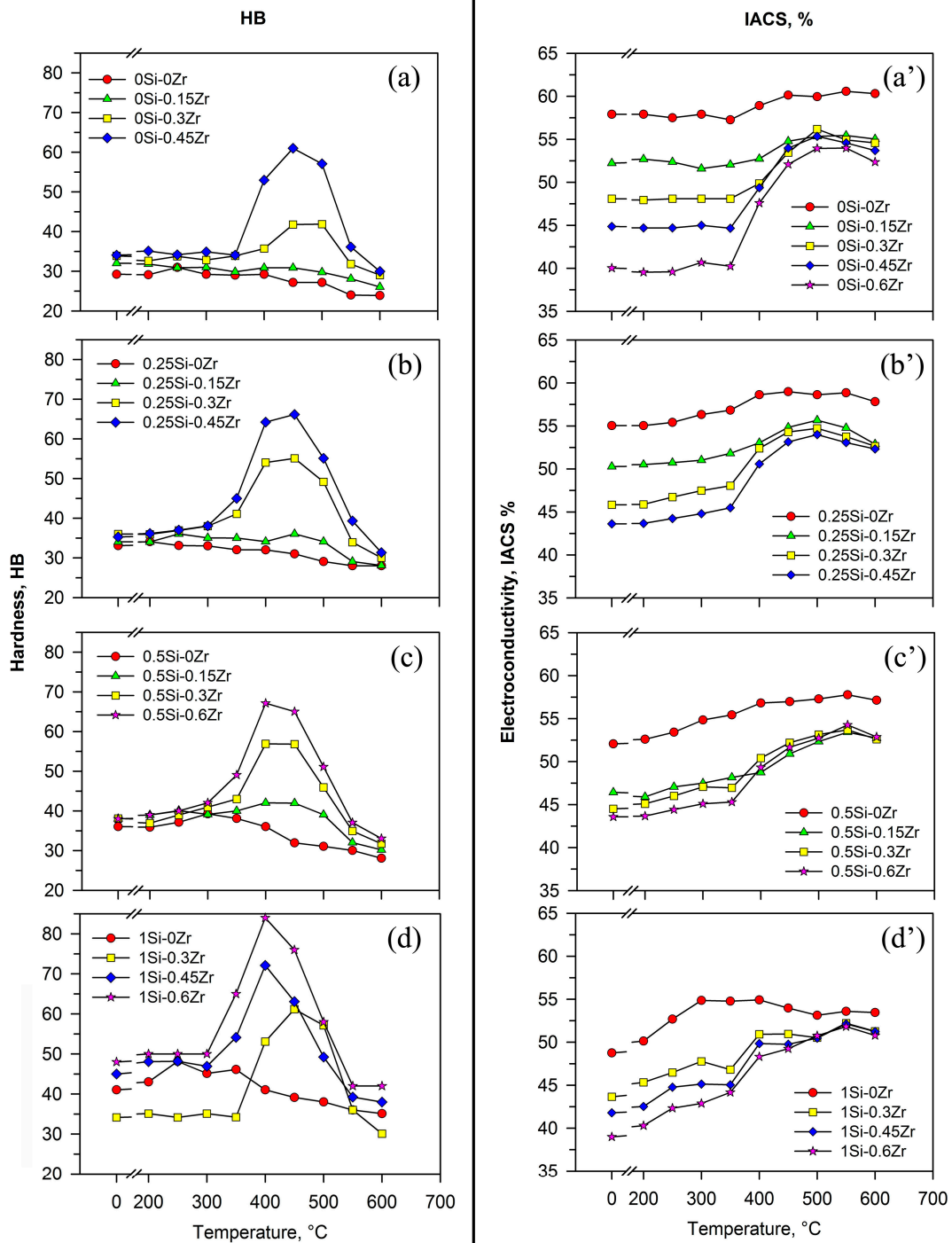


Figure 7. Temperature dependence of the microhardness (a–d) and the electrical conductivity (a–d’) for Al-1% Fe-Si-Zr alloys with a fixed content of Si and different contents of Zr: (a, a’) 0 wt. % Si; (b, b’) 0.25 wt. % Si; (c, c’) 0.5 wt. % Si; (d, d’) 1.0 wt. % Si.

The Zr content leads to an increase in the hardness of the studied alloys. There are no significant changes in the hardness with an increase in the temperature up to 350 °C. The highest hardness is observed in the temperature range from 400 °C to 450 °C. A further increase in the annealing temperature up to 600 °C is accompanied by a decrease in the hardness. Note that the peak-hardness of the Al-Fe-Si-Zr alloys that determines the collective Si and Zr influence improves with its content increase.

The effect of Si and Zr content on the electrical conductivity is presented in Figure 7a'–d'. The increase of Si-content led to the electrical conductivity degradation of as-cast, as well as annealed alloys. The increase of the annealing temperature is accompanied by the small electrical conductivity improvement. The peak electrical conductivity decreases with the increase of Si content, as well. The electrical conductivity decreases significantly with an increase in the Zr content in the temperature range from 20 °C to 350 °C. The highest electrical conductivity was also observed at the range from 450 °C to 500 °C. A further increase in the testing temperature up to 500 °C is accompanied by an increase in the conductivity.

4. Discussion

Figures 4 and 5 show that the annealing promoted the phase transformation from the metastable Al_6Fe or $\alpha-AlFeSi$ to the Al_3Fe equilibrium phase and induced a significant change in solute levels in the solid solution. The SEM investigation of the studied Al-Fe-Si-Zr alloys demonstrates that the Fe-containing intermetallics in Al-Fe-Si alloys are both of the so-called α -phases forming the Chinese script-like morphology and sometimes even as polyhedral crystals, as shown in [15,16].

Most of the Fe combines with both aluminum and Si to form secondary intermetallic phases because of the low solid solubility of Fe in aluminum (i.e., max. 0.05% at 650 °C). The equilibrium intermetallic Al_3Fe phase can form at slow solidification rates. However, depending on the alloy composition, cooling rate and presence of trace elements, a wide range of intermediate intermetallic phases, such as Al_mFe , Al_9Fe , Al_6Fe , Al_xFe and $\alpha-AlFeSi$ (Al_8Fe_2Si), can form and are considered metastable Fe-rich phases in the literature [17,18].

An increase in the Si content leads to an acceleration of the solid solution decomposition and its maximum replacement to the lower temperature region (Figure 8). A further increase in Si content did not lead to a change in the speed and temperature of the described peak, so the Si content equal to 0.25 wt. % provides the best combination of hardness and electrical conductivity. The same effect of Si has been described also in [11].

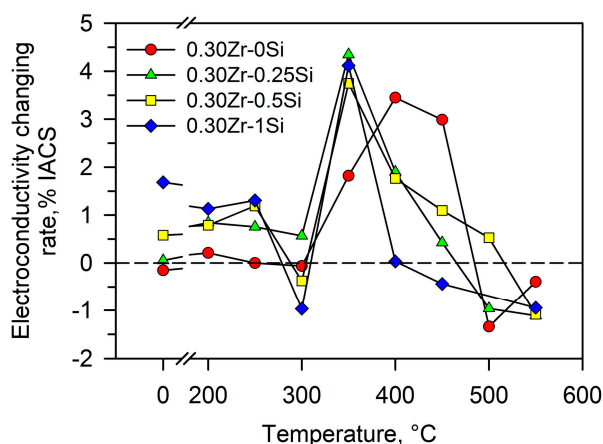


Figure 8. Temperature dependence of the electrical conductivity change of Al-1% Fe-Si-0.3% Zr alloys.

It should be noted that the electrical conductivity of the studied alloys without Zr varies insignificantly in all investigated temperature ranges. An increase in the Si content led to a decrease in

the electrical conductivity of the investigated alloys. By contrast, an increase in the Si content led to an increase in the hardness, as shown in Figure 7. The high content of Si should have led to the formation of Si-inclusion in the structure (Figure 3d) and contributed to a decrease in the electrical conductivity of the alloys, as can be seen in Figure 8c,d. The negative effects of Si on the Al alloys' properties are described in the literature [19]. Thus, the addition of the Si in the Al-1% Fe alloy leads to the increase of the hardness, while the electrical conductivity decreases, as can see in Figure 7.

It is known that Zr exists in four forms at different heat processing and heat-treatment stages, i.e., solid solution in matrix, coarse primary Al_3Zr phase, metastable Al_3Zr phase, as well as equilibrium Al_3Zr phase [20]. SEM and TEM micrographs in Figure 5 show the small spheroidal coherent Al_3Zr ($L1_2$) precipitates in the dendritic cells surrounded by precipitate-free interdendritic channels. An increase in the Zr content of more than 0.3 wt. % leads to the formation of primary Al_3Zr particles in the as-cast structure and negatively affects the properties of the investigated alloys. The same results are reported in [21–23]. Furthermore, the appearance of the primary Al_3Zr can also be associated with such disadvantages of the alloy production regime as casting temperature and cooling rate. In the cast structure of the investigated alloys with 0.45–0.6 wt. % Zr, there are primary Al_3Zr crystals, which on the one hand speaks to an insufficient cooling rate ensuring the entry of Zr into the solid solution of aluminum. It is also obvious that the formation of primary Al_3Zr particles leads to a decrease of the volume fraction of secondary precipitations of Al_3Zr (nanoparticles), which negatively affect the thermal stability according to the Zener drag force equation [24].

It is clearly seen in Figure 4 that Al_3Zr precipitates are forming at the interdendritic channels that result from Zr segregation at the dendrite cores. Thus, dendritically-distributed Al_3Zr precipitates are also a significant problem in commercial wrought alloys, where Zr is added as a recrystallization inhibitor.

The strong age hardening response of the Zr-containing alloy is due to the precipitation of small (10 nm) coherent Al_3Zr ($L1_2$) precipitates, shown by SEM (Figure 4b,c) and TEM (Figure 5). The decrease in the hardness with an increase in temperature can be explained by the precipitation hardening due to the Orowan mechanism. The shear stress required for a dislocation to loop around a precipitate particle is inversely proportional to the edge-to-edge distance between the particles, which was first described by Orowan as shown in Equation (1) [25]:

This is an example of the equation:

$$\Delta\tau = G_B/L, \quad (1)$$

where G_B is the Burgers vector and L is the distance between two particles. According to Equation (1), the strengthening effect from the metastable nanoscale Al_3Zr $L1_2$ dispersoids with an average size of 10 nm was 17-times higher compared to the stable incoherent plate-like D0_{23} Al_3Zr particles with a length equal to 200 nm and a thickness of about 50 nm (Figure 6). Kendig et al. also reported that the maximum hardening is achieved with the size of precipitates Al_3Zr at 5–10 nm [26].

Figure 8 depicts that the electrical conductivity decreases significantly with an increase in the Zr content in the range from 20 °C to 350 °C. By contrast, a further increase in the testing temperature up to 500 °C is accompanied by an increase in the electrical conductivity. This increase in the electrical conductivity with an increasing in temperature can be explained by the decomposition of the solid solution and the diffusion of Zr atoms into particles leading to a decrease of the number of point defects in the matrix, less electron scattering and a decrease in the electrical conductivity. Furthermore, an increase in the Si amount leads to the movement in the maximum of the observed curves to the lower temperature region, which means a decrease in the temperature of the solution decomposition.

The structural and phase transformations during the annealing process were estimated through conductivity and hardness measurements. It is well known that Zr dissolved in α (Al) strongly reduces electrical conductivity. Belov et al. presented the influence of annealing cycles up to 650 °C on the specific conductivity and hardness (HV) of hot-rolled sheets of Al alloys containing up to 0.5 wt. % Zr (mass fraction). It is demonstrated that the conductivity depends on the content of Zr in the Al solid solution, which is the minimum after holding at 450 °C for 3 h. On the other hand, the hardness

of the alloy is mainly caused by the amount of nanoparticles of the L_{12} (Al_3Zr) phase that defines the retention of strain hardening. Chen et al. described an aluminum alloy with 1 wt. % of Zr and 1.7 wt. % of V, which gives an increase to about 5 vol. % of the metastable L_{12} phase after aging. It is known that the formation of stable incoherent particles is unexpected and undesirable as this meant that there was less Zr available in the solid solution to form nanoscale secondary Al_3Zr precipitates, which are desirable in order to limit grain growth.

It can be seen in Figure 7 that the best combination of electrical conductivity and hardness values can be reached with an acceptable holding time at a temperature of about 450 °C. Electrical conductivity reaches the maximum value at 450 °C and can be explained by the maximum depletion of Zr from the Al solid solution, as was shown in our previous work [17,27]. The maximum electrical conductivity is ensured by all the Zr in Al_3Zr particles. It can be realized using the high-temperature S600 annealing. However, use of the lower annealing temperatures in view of providing the optimal hardening due to the formation of the metastable nanosized Al_3Zr is also necessary. However, the decomposition of the solid solution at 350 °C required more than 100 h for the slow diffusion of Zr in aluminum according to Knipling [7,18]. It should be noted that conductivity strongly depends not only on the temperature of the annealing, but also on the holding time, as well. Al-Mg-Zr alloys with an ultrafine-grained microstructure combined with a high electrical conductivity (over 57% The International Annealed Copper Standard) after annealing, severe plastic deformation (SPD) via equal channel angular pressing-conforming (ECAP-C), followed by cold drawing have been also described in detail in [25].

Thus, the content of Si and Zr provides the best combination (conjunction) of hardness and electrical conductivity of Al-1% Fe-Si-Zr alloys as can be clearly seen from the summary graphs shown in Figure 9. A compromise of the high conductivity and hardness can be achieved if the temperature of heat treatment is in the range of 450 °C–500 °C and the content of the Si 0.25 wt. %–0.50 wt. %, with the Zr content no more than 0.3 wt. %, respectively, as can be concluded from the obtained results.

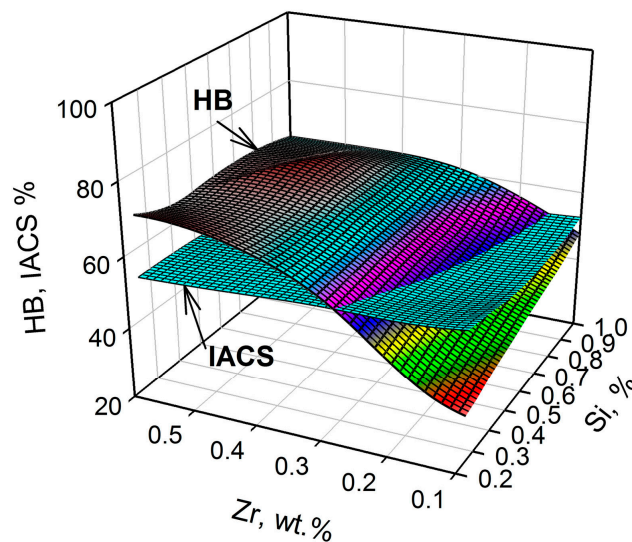


Figure 9. Complex effect of Si and Zr on the electrical conductivity (The International Annealed Copper Standard (IACS)) and hardness (HB) of the Al-1% Fe-Si-Zr alloys.

5. Conclusions

In summary, the relationships between the hardness and electrical conductivity were examined for several Al-Si-Fe-Zr alloys. The influence of the annealing temperature and chemical composition on the microstructure, electrical conductivity and hardness of Al-Fe-Si-Zr alloys with a different content

of Si ranging from 0 wt. % to 1 wt. %, various content of Zr from 0 wt. % to 0.6 wt. % and fixed content of Fe of 1 wt. % has been studied in the present work. The following results were obtained:

1. The $\text{Al}_8\text{Fe}_2\text{Si}$ phase with a Chinese script-like morphology was formed for the investigated alloy at 0.25 wt. % of Si, which ensures manufacturability with possible further deformation. An increase in the Si content leads to an increase of Si content in the solid solution and negatively affects the electrical conductivity of the alloys and increases the hardness. Therefore, the favorable content of Si was equal to 0.25 wt. %–0.50 wt. %. It was also described that Si accelerates the decomposition of the solid solution for alloys with a content of Zr equal to 0.3 wt. %.

2. An increase in the content of Zr over 0.3 wt. % in the investigated alloys leads to the formation of the primary Al_3Zr particles, which substantially reduce the hardness; while, 0.15 wt. % of Zr was insufficient for the formation of the secondary Al_3Zr precipitates. The microstructure evaluation showed that with an increase in the amount of Zr from 0.15 wt. % to 0.3 wt. %, an increase in the amount of Al_3Zr dispersoids in the dendrites was observed. The microstructure of the considered alloys with a fixed content of Si equal to 0.5 wt. % and Fe equal to 1 wt. % mostly consists of the solid solution of aluminum (Al) and a eutectic $\text{Al}_8\text{Fe}_2\text{Si} + (\text{Al})$ along the boundaries of dendritic cells. Therefore, the preferable content of Zr was equal to 0.3 wt. %.

3. It was shown that an increase in the Zr content led to an increase in the hardness of the studied alloys. The highest hardness is observed after annealing at 450 °C. A further increase of the temperature leads to a decrease in the hardness.

4. It was clearly shown that small coherent Al_3Zr (L_{12}) precipitates formed in the Al-1% Fe-0.25% Si-0.3% Zr alloy after S450 annealing. The maximum hardness of the investigated alloy was observed after S450 annealing because of the maximum strengthening effect due to the formation of these particles. It was shown that these particles are effective barriers to grain-boundary migration according to Orowan and transformed into stable incoherent Al_3Zr (D_{023}) precipitates after S600 annealing. The loss of the coherence of Al_3Zr particles led to a decrease in the hardness.

Acknowledgments: The financial support received from the Ministry of Education and Science, Russia, (Belgorod State University Project No. 03.G25.31.0278) is acknowledged. The main results were obtained by using the equipment of the Joint Research Center, «Technology and Materials», Belgorod State National Research University.

Author Contributions: Nikolay Belov and Natalya Korotkova contributed material and realized the electrical conductivity and microhardness testing. Anna Mogucheva, Anna Morozova, Dmitriy Bukin and Olga Lukianova proposed and performed microstructure experiments and realized the data processing. Anna Mogucheva, Anna Morozova and Rustam Kaibyshev discussed and analyzed the obtained results.

Conflicts of Interest: The authors declare no conflict of interest.

References

1. GencalpIrizalp, S.; Saklakoglu, N. Effect of Fe-rich intermetallics on the microstructure and mechanical properties of thixoformed A380 aluminum alloy. *Eng. Sci. Technol. Int. J.* **2014**, *17*, 58–62. [[CrossRef](#)]
2. Belov, N.A.; Alabin, A.N.; Eskin, D.G.; Istomin-Kastrovskii, V.V. Optimization of hardening of Al–Zr–Sc cast alloys. *J. Mater. Sci.* **2006**, *41*, 5890–5899. [[CrossRef](#)]
3. Mondolfo, L.F. *Aluminum alloys: Structure and Properties*; Butterworths: London, UK, 1976; ISBN 9781483144825.
4. Panahi, D. *Precipitation of Intermetallic Phases from Rapidly Solidifying Aluminum Alloys*; McMaster University: Hamilton, ON, Canada, 2009.
5. Kral, M.V.; Nakashima, P.N.H.; Mitchell, D.R.G. Electron microscope studies of Al-Fe-Si intermetallics in an Al-11 Pct Si alloy. *Metall. Mater. Trans. A* **2006**, *37*, 1987–1997. [[CrossRef](#)]
6. Ryum, N. Precipitation and recrystallization in an Al-0.5 wt % Zr-alloy. *Acta Metall.* **1969**, *17*, 269–278. [[CrossRef](#)]
7. Knipling, K.E.; Dunand, D.C.; Seidman, D.N. Precipitation evolution in Al–Zr and Al–Zr–Ti alloys during aging at 450–600 °C. *Acta Mater.* **2008**, *56*, 1182–1195. [[CrossRef](#)]
8. Belov, N.A.; Alabin, A.N. Energy Efficient Technology for Al–Cu–Mn–Zr Sheet Alloys. *Mater. Sci. Forum* **2013**, *765*, 13–17. [[CrossRef](#)]

9. Alabin, A.N.; Belov, A.N.; Korotkova, N.O.; Samoshina, M.E. Effect of annealing on the electrical resistivity and strengthening of low-alloy alloys of the Al-Zr-Si system. *Metal Sci. Heat Treat.* **2016**, *58*, 527–531. [[CrossRef](#)]
10. Belov, N.A.; Alabin, A.N.; Prokhorov, A.Y. Effect of zirconium additive on the strength and electrical resistivity of cold-rolled aluminum sheets. *Izv. Vysh. Uchebn. Zaved. Tsvetn. Met.* **2009**, *4*, 42–47.
11. Belov, N.A.; Aksenov, A.A.; Eskin, D.G. *Iron in Aluminium Alloys: Impurity and Alloying Element*; Taylor and Francis: London, UK, 2002; pp. 1107–1112. ISBN 0-415-27352-8.
12. Vorontsova, L.A.; Maslov, V.V.; Peshkov, I.B. *Aluminum and Aluminum Alloys in Electrical Products*; Energiya: Moscow, Russia, 1971. (In Russian)
13. Popovic, S.; Grzeta, B.; Ilakovac, V.; Kroggel, R.; Wendrock, G.; Löffler, H. Lattice constant of the FCC Al-rich α -Phase of Al-Zn alloys in equilibrium with GP zones and the β (Zn)-Phase. *Phys. Status Solidi A* **1992**, *130*, 273–292. [[CrossRef](#)]
14. Ma, Y.; Romming, C.; Lebech, B.; Gjønnes, J.; Taftø, J. Structure refinement of Al₃Zr using single-crystal X-ray diffraction, powder neutron diffraction and CBED. *Acta Crystallogr. B* **1992**, *48*, 11–16. [[CrossRef](#)]
15. Shakiba, M.; Parson, N.; Chen, X.-G. Effect of homogenization treatment and silicon content on the microstructure and hot workability of dilute Al-Fe-Si alloys. *Mater. Sci. Eng. A* **2014**, *619*, 180–189. [[CrossRef](#)]
16. Taylor, J.A. Iron-Containing intermetallic phases in Al-Si based casting alloys. *Procedia Mater. Sci.* **2012**, *1*, 19–33. [[CrossRef](#)]
17. Liu, P.; Thorvaldsson, T.; Dunlop, G.L. Formation of intermetallic compounds during solidification of dilute Al-Fe-Si alloys. *Mater. Sci. Technol.* **1986**, *2*, 1009–1018. [[CrossRef](#)]
18. Skjerpe, P. Intermetallic phases formed during DC-casting of an Al-0.25 Wt Pct Fe-0.13 Wt Pct Si alloy. *Metall. Mater. Trans. A* **1987**, *18*, 189–200. [[CrossRef](#)]
19. Belov, N.A.; Alabin, A.N.; Matveeva, I.A.; Eskin, D.G. Effect of Zr additions and annealing temperature on electrical conductivity and hardness of hot rolled Al sheets. *Trans. Nonferrous Met. Soc. China* **2015**, *25*, 2817–2826. [[CrossRef](#)]
20. Zhang, J.; Ding, D.; Zhang, W.; Kang, S.; Xu, X.; Gao, Y.; Chen, G.; Chen, W.; You, X. Effect of Zr addition on microstructure and properties of Al-Mn-Si-Zn-based alloy. *Trans. Nonferrous Met. Soc. China* **2014**, *24*, 3872–3878. [[CrossRef](#)]
21. He, Y.; Zhang, X.; Cao, Z. Effect of minor Sc and Zr addition on grain refinement of as-cast Al-Zn-MgCu alloys. *Chin. Foundry* **2009**, *6*, 214–218.
22. Garcia, D.A.; Dye, D.; Jackson, M.; Grimes, R.; Dashwood, R.J. Development of microstructure and properties during the multiple extrusion and consolidation of Al-4Mg-1Zr. *Mater. Sci. Eng. A* **2010**, *527*, 3358–3364. [[CrossRef](#)]
23. Zhang, L.; Eskin, D.G.; Miroux, A.G.; Katgerman, L. On the mechanism of the formation of primary intermetallics under ultrasonic melt treatment in an Al-Zr-Ti alloy. *IOP Conf. Ser. Mater. Sci. Eng.* **2012**, *27*, 012002. [[CrossRef](#)]
24. PA, M.; Ferry, M.; Chandra, T. Five decades of the Zener equation. *ISIJ Int.* **1998**, *38*, 913–924. [[CrossRef](#)]
25. Hull, D.; Bacon, D.J. *Introduction to Dislocations*; Butterworth-Heinemann: Oxford, UK, 1984; ISBN 0750623618.
26. Kendig, K.; Miracle, D. Strengthening mechanisms of an Al-Mg-Sc-Zr alloy. *Acta Mater.* **2002**, *50*, 4165–4175. [[CrossRef](#)]
27. Murashkin, M.Y.; Medvedev, A.E.; Kazykhanov, V.U.; Raab, G.I.; Ovid'ko, I.A.; Valiev, R.Z. Microstructure, strength, electrical conductivity and heat resistance of an Al-Mg-Zr alloy after ECAP-conform and cold drawing. *Rev. Adv. Mater. Sci.* **2016**, *47*, 16–25.

